JOURNAL OF GUIDANCE, CONTROL, AND DYNAMICS
Vol. 36, No. 1, January–February 2013

Time-Optimal Path Following for Fixed-Wing Aircraft

Yiming Zhao*
Mitsubishi Electric Research Laboratories, Cambridge, Massachusetts 02139
and
Panagiotis Tsiotras†
Georgia Institute of Technology, Atlanta, Georgia 30332-0150

DOI: 10.2514/1.57471

In this paper, a method is proposed for the minimum-time travel of a fixed-wing aircraft along a prescribed geometric path. The method checks the feasibility of the path, namely, whether it is possible for the aircraft to travel along the path without violating the state or control constraints. If the path is feasible, the method subsequently finds a semi-analytical solution of the speed profile that minimizes the travel time along the path. The optimal speed profile is then used to time parameterize the path and generate the state trajectory along with the control histories via inverse dynamics. Two algorithms for the time-optimal parameterization are proposed. Numerical examples are presented to demonstrate the validity, numerical accuracy, and optimality of the proposed method.

Nomenclature

C_D	=	drag coefficient
C_{D_0}	=	zero lift drag coefficient
C_L	=	lift coefficient
C_L^*	=	optimal lift coefficient
$C_{L_{\max}}$	=	maximum lift coefficient
$C_{L_{\min}}$	=	minimum lift coefficient
E	=	kinetic energy per unit mass, J/Kg
E^*	=	optimal specific kinetic energy, J/Kg
g	=	gravity acceleration, m/s^2
$\bar{g}_w$	=	upper bound of kinetic energy, J/Kg
$\underline{g}_w$	=	lower bound of kinetic energy, J/Kg
K	=	induced drag coefficient
$\mathcal{K}$	=	intervals with active speed constraint
$\mathcal{K}_L$	=	intervals with active minimum speed constraint
$\mathcal{K}_U$	=	intervals with active maximum speed constraint
m	=	mass, kg
S	=	wing surface area, m^2
$\mathcal{S}_j^+$	=	forward specific kinetic energy integrals, J/kg
$\mathcal{S}_j^-$	=	backward specific kinetic energy integrals, J/kg
s	=	path coordinate, m
s_f	=	path length, m
T	=	thrust, N
T^*	=	optimal thrust, N
$T_{\max}$	=	maximum thrust, N
$T_{\min}$	=	minimum thrust, N
$\bar{T}_w$	=	thrust for maximum speed travel, N
$\underline{T}_w$	=	thrust for minimum speed travel, N
t	=	time, t_f final time, s
$\mathcal{W}$	=	admissible velocity set
x, y, z	=	position, m
γ	=	path angle, rad
Δ_r	=	relative position error
λ	=	costate variable
v	=	speed, m/s
ρ	=	air density, kg/m^3 ϕ bank angle, rad
ϕ^*	=	optimal bank angle, rad
$\phi_{\max}$	=	maximum bank angle, rad
$\phi_{\min}$	=	minimum bank angle, rad ψ heading angle, rad

I. Introduction

OPTIMAL control techniques allow the computation of optimal (and hence feasible) aircraft trajectories using realistic dynamics, subject to state and control constraints [1–4]. Such approaches are based necessarily on the numerical solution of the optimal control problem. Although such purely numerical solutions can deal with high-fidelity aircraft models, they are typically plagued by convergence issues, and they are thus not amenable to onboard and real-time implementation. The convergence of the solution depends heavily on the quality of the initial guess of the time histories of both the state and control variables. A good initial guess can help the solution converge much faster. A bad initial guess will hinder convergence or even lead to divergence of the overall numerical scheme. In general, it is not easy to obtain a set of state and control histories that are consistent with the aircraft dynamics and that satisfy the given constraints and boundary conditions. In addition, optimal control solutions based completely on numerics do not offer any useful insights about the problem itself. Such insights are possible only through a detailed analysis of the optimality conditions, which can reveal the optimal switching structure of the problem.

In this paper, an alternative approach is proposed to compute minimum-time suboptimal aircraft trajectories. Borrowing ideas from the motion-planning literature, the optimal trajectory generation problem is divided into two separate, albeit closely related, layers. At the first layer, an obstacle-free, geometric path to be followed by the aircraft is computed. In the second layer, the optimal velocity profile is found for the aircraft to follow the given path in minimum time such that the state and control constraints are satisfied. This problem decomposition bypasses the solution of the complete time-optimal control problem and is numerically very efficient. Because both the optimal path generation problem and the time-parameterization problem can be computed very efficiently, replanning can be used to search for the actual optimal trajectory by locally modifying the original path [5,6]. Because there is a plethora of algorithms to construct obstacle-free geometric paths in the configuration space [7–10], in this paper, we will deal exclusively with the optimal velocity profile generation layer. The resulting reduction in the problem dimensionality allows one to analyze in great detail the necessary optimality conditions and hence characterize the optimal switching structure for this problem.

Apart from its utility as a stand-alone approach to generate feasible minimum-time suboptimal paths in a numerically efficient manner, the proposed method can also be used to construct good initial

Presented as Paper 2010-3352 at the AIAA Infotech@Aerospace 2010, Atlanta, Georgia, 20–22 April 2010; received 28 December 2011; revision received 1 May 2012; accepted for publication 7 May 2012; published online 4 December 2012.

*Adjunct Member Research Stuff; yzhao7@gatech.edu.
†College of Engineering Dean's Professor, School of Aerospace Engineering; tsiotras@gatech.edu. Fellow AIAA.

guesses for a complete trajectory optimization solver, thus helping improve their convergence rate [11].

The hierarchical decomposition of the feasible trajectory generation problem to a geometric and kino-dynamic layer is well known in the motion-planning literature, where several methods, including concatenations of Dubins's path primitives, potential field methods, etc., have been used to construct obstacle-free geometric paths in the configuration space [7–10]. These approaches typically do not provide the control histories required for maneuvering the vehicle to follow the given path. Instead, the actual implementation (i.e., path following) is left to a trajectory tracking controller (or human pilot), which generates the required control commands to follow the path after a suitable time parameterization along the geometric path is imposed. However, because most of these path-planning methods are at the kinematic level, they do not account for the dynamics of the aircraft, and hence the feasibility of the resulting trajectory is not guaranteed a priori. In other words, it is possible that no control exists that allows the aircraft to follow the proposed path without violating the control or state constraints. The methodology proposed in this paper remedies this inconsistency by checking the feasibility of the given path, based on the given state and control constraints. Hence, it can be used equally well as a postprocessing tool for pure geometric/kinematic planners for checking the feasibility of the generated path. Specifically, the approach may be used as a bridge between geometric path-planning methods and numerical optimal control methods to improve convergence of a nonlinear programming (NLP) solver. The geometric path given by the geometric planner can be optimally time parameterized to obtain the corresponding state and control histories, which can then be passed to the NLP solver as an initial guess. Compared with other feasible initial guess generation methods, however, such as [12], the method introduced in this paper seeks not only feasibility but also optimality of the time-parameterized path.

It should be pointed out that the problem of the time parameterization along a given geometric path has been extensively analyzed in robotics literature. For the case of robotic manipulators, for instance, it has been shown that the control is bang–bang when the speed limit is not active [13]. In this paper, it will be shown that a similar result holds for the optimal thrust input of a fixed-wing aircraft following an a priori given path in minimum time. Although the bang–bang form of the control for robotic manipulators has been proved in [13], the switching structure between the upper and lower control bounds has not been studied, despite the fact that the appropriate structure has been used implicitly in the algorithms proposed in [13–17]. References [14–17] take advantage of the Lagrangian form of the dynamics of a fully actuated robotic manipulator to compute the required speed profile for the manipulator to move along a specified path in minimum time. In this paper, the switching structure of the optimal thrust profile is completely characterized using the necessary conditions for optimality resulting from the application of Pontryagin's maximum principle.

The contributions of the paper can be summarized as follows: First, it is shown that the problem of the optimal time parameterization of a geometric path for a fixed-wing aircraft can be converted to a constrained *scalar* functional optimization problem by decoupling the controls. Analytical expressions of the aircraft allowable velocity region are provided. This feasibility region is characterized by the imposed constraints, such as the bank angle and lift coefficient constraints. Second, a semi-analytic solution to this scalar optimal control problem is obtained by applying Pontryagin's maximum principle. Specifically, the optimal switching structure is characterized. Third, two algorithms are presented for generating the optimal speed profile, and hence also the profile of the optimal thrust, in a numerically efficient manner. Finally, it is shown using numerical examples that the developed theory can be used to construct the optimal solution. By comparing the results against the optimal solution obtained by a standard NLP solver, it is shown that the proposed methodology indeed predicts the optimal switching structure.

II. Aircraft Model

Let a path in the three-dimensional space, parameterized by the path coordinate s, be given as follows: $x = x(s)$, $y = y(s)$, $z = z(s)$, where $s \in [s_0, s_f]$. The main objective of this paper is to find a time parameterization along the path, that is, a function $s(t)$, where $t \in [0, t_f]$ such that the corresponding time-parameterized trajectory $[x(s(t)), y(s(t)), z(s(t))]$ minimizes the flight time t_f. It is assumed that $x(s)$, $y(s)$, and $z(s)$ are continuously differentiable and piecewise analytic.[‡]

Consider the following equations of motion for a point-mass model of a fixed-wing aircraft [19]:

$$\dot{x} = v \cos\gamma \cos\psi \tag{1}$$

$$\dot{y} = v \cos\gamma \sin\psi \tag{2}$$

$$\dot{z} = v \sin\gamma \tag{3}$$

$$\dot{v} = \frac{1}{m}[T - F_D(C_L, v, \rho) - mg \sin\gamma] \tag{4}$$

$$\dot{\gamma} = \frac{1}{mv}[F_L(C_L, v, \rho)\cos\phi - mg \cos\gamma] \tag{5}$$

$$\dot{\psi} = -\frac{F_L(C_L, v, \rho)\sin\phi}{mv\cos\gamma} \tag{6}$$

where x, y, z are the coordinates defining the position of the aircraft, v is the speed, ρ is the air density (varying with altitude), γ is the flight-path angle, ψ is the heading angle, and ϕ is the bank angle. In this model, the lift coefficient C_L, the bank angle ϕ, and the thrust T are the control inputs. The aerodynamic lift force $F_L(C_L, v, \rho)$ and drag force $F_D(C_L, v, \rho)$ are given by

$$F_L(C_L, v, \rho) = \frac{1}{2}\rho v^2 S C_L$$

$$F_D(C_L, v, \rho) = \frac{1}{2}\rho v^2 S C_D = \frac{1}{2}\rho v^2 S(C_{D_0} + K C_L^2)$$

where C_{D_0} and K are parameters describing the aerodynamics of the aircraft, and S is the main wing surface area. In general, C_{D_0} and K depend continuously on the Mach number. Henceforth, it will be assumed that C_{D_0} and K are continuous functions of the airspeed and the path length s.

Because the given path is naturally parameterized using the path coordinate s instead of time, the equations of motion can be rewritten with respect to s as follows (where the prime denotes differentiation with respect to s):

$$x' = \cos\gamma \cos\psi \tag{7}$$

$$y' = \cos\gamma \sin\psi \tag{8}$$

$$z' = \sin\gamma \tag{9}$$

$$v' = \frac{1}{mv}[T - F_D(C_L, v, \rho) - mg \sin\gamma] \tag{10}$$

$$\gamma' = \frac{1}{mv^2}[F_L(C_L, v, \rho)\cos\phi - mg \cos\gamma] \tag{11}$$

$$\psi' = -\frac{F_L(C_L, v, \rho)\sin\phi}{mv^2\cos\gamma} \tag{12}$$

where the following relations have been used for deriving Eqs. (7–12):

[‡]A function is *piecewise analytic* if it is defined on a collection of subintervals, such that its restriction on the closure of each subinterval (possibly after continuation) is analytic [18]. This is a rather weak assumption. Concatenations of piecewise polynomials or spline functions, for example, satisfy these conditions. Note that this definition allows for a piecewise analytic function to be discontinuous at the boundaries of the subintervals; at these points, however, the limits from the left and the right of the function and its higher order derivatives exist.

$$\mathrm{d}t = \frac{\mathrm{d}s}{v} \tag{13}$$

$$\mathrm{d}s = \sqrt{\mathrm{d}^2x + \mathrm{d}^2y + \mathrm{d}^2z} \tag{14}$$

$$\psi = \arctan\frac{\mathrm{d}y}{\mathrm{d}x} = \arctan\frac{y'}{x'} \tag{15}$$

$$\gamma = \arctan\frac{\mathrm{d}z}{\sqrt{\mathrm{d}x^2 + \mathrm{d}y^2}} = \arctan\frac{z'}{\sqrt{x'^2 + y'^2}} \tag{16}$$

$$\psi' = \frac{1}{1 + (y'/x')^2}\frac{y''x' - y'x''}{x'^2} = \frac{x'^2}{x'^2 + y'^2}\frac{y''x' - y'x''}{x'^2} = \frac{y''x' - y'x''}{x'^2 + y'^2} \tag{17}$$

$$\gamma' = \frac{z''x'^2 + z''y'^2 - z'x''x' - z'y''y'}{\sqrt{x'^2 + y'^2}} \tag{18}$$

Note that the flight-path angle γ and the heading angle ψ are purely geometric variables. Therefore, once a three-dimensional path $[x(s), y(s), z(s)]$ is given, these variables and their derivatives with respect to the path coordinate can be computed from Eqs. (17) and (18). It is clear from the previous expressions that the continuous differentiability of x, y, z implies the continuity of x', y', and z'. It is also assumed that the fixed-wing aircraft flight-path angle is always between $-\pi/2$ and $\pi/2$, a reasonable assumption for civil fixed-wing aircraft, which are the main focus of this paper. Note that x'', y'', z'', γ', ψ', and v' are allowed to be discontinuous.

To time parameterize an arbitrary path, it is sufficient to obtain the history of the speed $v(s)$ with respect to the path coordinate s. After the optimal speed profile $v^*(s)$ is obtained, the corresponding optimal time-parameterized trajectory can be calculated by integrating Eq. (13). Specifically, let $t^*: [s_0, s_f] \to [0, t_f]$ be the bijective mapping between the path coordinate and the corresponding time coordinate along the optimal solution. Then $t^*(s)$ denotes the time at which the aircraft arrives at the position corresponding to the path coordinate s. Since $\mathrm{d}t^* = \mathrm{d}s/v^*(s)$, it follows that the optimal time profile along the path is given by

$$t^*(s) = \int_{s_0}^{s} \mathrm{d}t^* = \int_{s_0}^{s} 1/v^*(s)\,\mathrm{d}s, \qquad s_0 \le s \le s_f$$

The optimal time parameterization of the geometric trajectory $(x(s), y(s), z(s))$ is then given by

$$(x^*(t), y^*(t), z^*(t)) = (x(t^{*-1}(t)), y(t^{*-1}(t)), z(t^{*-1}(t)))$$

It will be shown in Sec. V that the optimal thrust profile $T^*(s)$ along the path can be determined once $v^*(s)$ is known. Subsequently, the other controls can be recovered through inverse dynamics as follows:

$$\phi^*(s) = -\arctan\left(\frac{\cos\gamma(s)\psi'(s)}{\gamma'(s) + g\cos\gamma(s)/v^{*2}(s)}\right)$$

$$C_L^*(s) = \frac{2m}{\rho(s)S\cos\phi^*(s)}\left(\gamma'(s) + \frac{g\cos\gamma(s)}{v^{*2}(s)}\right)$$

Obviously, the key to the optimal time-parameterization along a geometric path is the optimization of the speed profile along the given path. Next, it will be shown how the state and control constraints of the problem can be mapped to a set of admissible velocity profiles in the $s - v^2/2$ plane. Later on, the optimal speed profile is found by solving a scalar functional optimization problem. The solution of the latter problem will provide the optimal time parameterization along the given path.

III. Admissible Kinetic Energy Set

It is required that the lift coefficient C_L, the bank angle ϕ, and the thrust T must stay within certain ranges during the whole flight, namely,

$$\begin{aligned} &C_L(s) \in [C_{L_{\min}}(s), C_{L_{\max}}(s)],\\ &\phi(s) \in [\phi_{\min}(s), \phi_{\max}(s)], T(s) \in [T_{\min}(s), T_{\max}(s)],\\ &\forall\ s \in [s_0, s_f] \end{aligned} \tag{19}$$

where $C_{L_{\min}}$, $C_{L_{\max}}$, $\phi_{\min}$, $\phi_{\max}$, $T_{\min}$, and $T_{\max}$ are piecewise analytic functions of s. These constraints account for limitations on the control inputs, which may vary along the path. It is also required that the aircraft speed satisfies the bounds $v(s) \in [v_{\min}(s), v_{\max}(s)]$, where $v_{\min}$ and $v_{\max}$ are piecewise analytic functions with $v_{\min}(s) > 0$ for all $s \in [s_0, s_f]$. It is further assumed that $C_{L_{\min}}(s) \le 0 \le C_{L_{\max}}(s)$, $-\pi/2 < \phi_{\min}(s) < 0 < \phi_{\max}(s) < \pi/2$, and $0 \le T_{\min}(s) < T_{\max}(s)$, for all $s \in [s_0, s_f]$, and that the flight-path angle satisfies $\gamma(s) \in (-\pi/2, \pi/2)$ for all $s \in [s_0, s_f]$. These are generic conditions for a civil fixed-wing aircraft in normal flight conditions and will help simplify notation and subsequent analysis. More general formulations of the bounds are possible. For example, the maximum thrust can be chosen as a function of both the airspeed and altitude [i.e., $T_{\max} = T_{\max}(v, s)$] without affecting the validity of the approach in this paper (see the numerical example in Sec. VI.A at the end of the paper). Such a constraint can be handled without changing the conclusions. For simplicity, however, the analysis in the next section assumes constant maximum thrust.

Let $E \triangleq v^2/2$ be the kinetic energy per unit mass of the aircraft. Also, let $E_{\max}(s) = v_{\max}^2(s)/2$ and $E_{\min}(s) = v_{\min}^2(s)/2$. In the sequel, the *specific kinetic energy* E will be used in lieu of the aircraft speed v to simplify the ensuing analysis. The constraint on the speed of the aircraft requires that $E_{\min}(s) \le E(s) \le E_{\max}(s)$ for all $s \in [s_0, s_f]$.

A. Lift Coefficient Constraint

From Eqs. (11) and (12), one obtains

$$\gamma' = \frac{1}{2m}\rho S C_L\cos\phi - \frac{g\cos\gamma}{v^2} \tag{20}$$

$$\psi' = -\frac{\rho v^2 S C_L\sin\phi}{2mv^2\cos\gamma} = -\frac{\rho S C_L\sin\phi}{2m\cos\gamma} \tag{21}$$

which can be rewritten as

$$C_L\cos\phi = \frac{2m}{\rho S}\left(\gamma' + \frac{g\cos\gamma}{v^2}\right) \tag{22}$$

$$C_L\sin\phi = -\frac{2m\psi'\cos\gamma}{\rho S} \tag{23}$$

Eliminating ϕ from Eqs. (22) and (23), and replacing v^2 with $2E$, one obtains

$$\begin{aligned} E &= g_1(C_L; \gamma, \gamma', \psi')\\ &\triangleq \frac{mg\cos\gamma}{\rho S}\left(\sqrt{C_L^2 - \left(\frac{2m\psi'\cos\gamma}{\rho S}\right)^2} - \frac{2m\gamma'}{\rho S}\right)^{-1} \end{aligned} \tag{24}$$

The other solution is omitted because it is always negative. Note that the constraint $0 < E_{\min}(s) \le E(s) \le E_{\max}(s) < \infty$ for all $s \in [s_0, s_f]$ implies that there exists $C_L(s) \in [C_{L_{\min}}(s), C_{L_{\max}}(s)]$ such that

$$0 < \sqrt{C_L^2(s) - \left(\frac{2m\psi'(s)\cos\gamma(s)}{\rho(s)S}\right)^2} - \frac{2m\gamma'(s)}{\rho(s)S} < \infty \tag{25}$$

for all $s \in [s_0, s_f]$. This is equivalent to the condition

$$\bar{C}_L(s) > \tilde{C}_L(s), \qquad \forall\, s \in [s_0, s_f] \tag{26}$$

where

$$\bar{C}_L(s) = \max\{-C_{L_{\min}}(s), C_{L_{\max}}(s)\} \tag{27}$$

and

$$\tilde{C}_L(s) = \begin{cases} \dfrac{2m}{\rho(s)S}|\psi'(s)|\cos\gamma(s), & \text{if } \gamma'(s) < 0 \\ \dfrac{2m}{\rho(s)S}\sqrt{\gamma'^2(s) + \psi'^2(s)\cos^2\gamma(s)}, & \text{if } \gamma'(s) \geq 0 \end{cases} \tag{28}$$

The given path $(x(s), y(s), z(s))$ is infeasible if Eq. (26) is not satisfied, owing to insufficient lift. When Eq. (26) holds, and because the right-hand side of Eq. (24) is a monotonically decreasing function with respect to C_L^2, the limits on the lift coefficient impose a lower bound on the kinetic energy E as follows:

$$E(s) \geq \underline{g}_{w1}(s) \triangleq \max\{E_{\min}(s), g_1(\bar{C}_L(s); \gamma(s), \gamma'(s), \psi'(s))\} \tag{29}$$

In other words, if the problem is feasible, Eq. (29) provides a lower bound on the allowable speed, whereas the bounds $C_{L_{\min}}(s) \leq C_L(s) \leq C_{L_{\max}}(s)$ on the lift coefficient do not impose any constraint on the maximum value of $E(s)$. Finally, note from Eq. (29) that, if $\underline{g}_{w1}(s)$ is unbounded, then the path is not feasible. Feasibility implies, in particular, that $\underline{g}_{w1}$ in Eq. (29) is a (possibly discontinuous) piecewise analytic function of s.

B. Bank Angle Constraint

To consider the effect of the bank angle constraint on the specific kinetic energy E, the lift coefficient C_L should be eliminated from Eqs. (22) and (23) to form an algebraic equation involving ϕ and E. However, two special cases need to be considered before proceeding with such an elimination: the case when $C_L(s) = 0$, and the case when $2\gamma'(s) + g\cos\gamma(s)/E(s) = 0$, for some $s \in [s_0, s_f]$.

If $C_L(s) = 0$ for some $s \in [s_0, s_f]$, then the lift is zero and the bank angle ϕ is indeterminate. In this case, the bounds $\phi_{\min}(s) \leq \phi(s) \leq \phi_{\max}(s)$ on the bank angle ϕ do not constrain the specific kinetic energy at s. Similarly, note that $2\gamma'(s) + g\cos\gamma(s)/E(s) = 0$ may hold only if $\gamma'(s) < 0$. If $2\gamma'(s) + g\cos\gamma(s)/E(s) = 0$, then $E(s)$ is uniquely determined, regardless of the value of the bank angle at s (i.e., the bank angle has no effect on E). Therefore, only the cases with $C_L(s) \neq 0$ and $2\gamma'(s) + g\cos\gamma(s)/E(s) \neq 0$ for some $s \in [s_0, s_f]$ need to be considered, leading to the following equation:

$$\tan\phi = -\frac{2\psi'\cos\gamma}{2\gamma' + g\cos\gamma/E} \tag{30}$$

Solving for E from Eq. (30) yields

$$E = g_2(\phi; \gamma, \gamma', \psi') \triangleq -\frac{1}{2}\frac{g\cos\gamma\tan\phi}{\gamma'\tan\phi + \psi'\cos\gamma} \tag{31}$$

The positivity of $E(s)$ requires that $g_2(\phi(s); \gamma(s), \gamma'(s), \psi'(s)) > 0$ for all $s \in [s_0, s_f]$, otherwise the path is infeasible. If $g_2(\phi; \gamma, \gamma', \psi') > 0$ along the given path, the constraints on E due to the bank angle bounds can be determined as follows:

1) When $\psi'(s) = 0$, Eq. (30) implies that $\phi(s) = 0$, and the bounds of ϕ impose no constraints on $E(s)$.

2) When $\psi'(s) \neq 0$, two cases need to be considered:

2a) If $\gamma'(s) = 0$, and since $\gamma \in (-\pi/2, \pi/2)$, it follows that $\cos\gamma \neq 0$, and

$$E(s) = g_2(\phi(s); \gamma(s), \gamma'(s), \psi'(s)) = -\frac{g\tan\phi(s)}{2\psi'(s)}$$

The condition $g_2(\phi(s); \gamma(s), \gamma'(s), \psi'(s)) > 0$ requires that $\phi(s)\psi'(s) < 0$. The constraint on ϕ then leads to the following upper bound on the specific kinetic energy E:

$$E(s) \leq \mu_0(s) \triangleq \max\left\{\frac{g\tan\phi_{\min}(s)}{2\psi'(s)}, \frac{g\tan\phi_{\max}(s)}{2\psi'(s)}\right\} \tag{32}$$

2b) If $\gamma'(s) \neq 0$, rewrite Eq. (31) as follows:

$$\gamma'(s)\tan\phi(s) + \psi'(s)\cos\gamma(s) = -\frac{g\cos\gamma(s)}{2E(s)}\tan\phi(s) \tag{33}$$

The bank angle constraint $\phi(s) \in [\phi_{\min}(s), \phi_{\max}(s)]$ limits the admissible value of $E(s)$ via Eq. (33). A necessary and sufficient condition for the satisfaction of this constraint is

$$\frac{g\cos\gamma(s)}{2E(s)} \leq \mu_1(s) \tag{34}$$

where $\mu_1(s) \triangleq \min\{h(s; \phi_{\min}, \gamma, \gamma', \psi'), h(s; \phi_{\max}, \gamma, \gamma', \psi')\}$ or

$$\frac{g\cos\gamma(s)}{2E(s)} \geq \mu_2(s) \tag{35}$$

where
$\mu_2(s) \triangleq \max\{-h(s; \phi_{\min}, \gamma, \gamma', \psi'), -h(s; \phi_{\max}, \gamma, \gamma', \psi')\}$, and where

$$h(s; \phi, \gamma, \gamma', \psi') \triangleq \gamma'(s) + \psi'(s)\cos\gamma(s)/\tan\phi(s) \tag{36}$$

To characterize the constraint on E induced by the bank angle, three subcases are analyzed and the results are given next:

2b.1) If $\mu_1(s) \leq 0$ and $\mu_2(s) \leq 0$, then Eq. (35) always holds as long as $E(s) > 0$.

2b.2) If $\mu_1(s) \leq 0$ and $\mu_2(s) > 0$, then Eq. (34) does not hold, and Eq. (35) must be satisfied, which is equivalent to the following constraint on $E(s)$:

$$E(s) \leq \frac{1}{2}g\cos\gamma(s)/\mu_2(s) \tag{37}$$

2b.3) Finally, if $\mu_1(s) > 0$, then it is required that either Eq. (37) holds, or the following inequality holds:

$$E(s) \geq \frac{1}{2}g\cos\gamma(s)/\mu_1(s) \tag{38}$$

Equations (32), (37), and (38) define the admissible values of $E(s)$ limited by the bank angle.

C. Summary of Algebraic Constraints

In the previous two sections it has been shown that the lift coefficient and the bank angle constraints can be reduced to a series of algebraic constraints on the value of the specific kinetic energy E along the path. Summarizing these results, for feasibility, the specific kinetic energy profile E must satisfy either one, or both, of the following two constraints. The first constraint is defined according to the inequalities

$$\underline{g}_{w1}(s) \leq E(s) \leq \bar{g}_{w1}(s), \qquad s \in [s_0, s_f] \tag{39}$$

where $\underline{g}_{w1}(s)$ from Eq. (29) and $\bar{g}_{w1}(s)$ from

$$\bar{g}_{w1}(s) \triangleq \begin{cases} \min\{E_{\max}(s), \mu_0(s)\}, & s \in \Gamma_1, \\ \min\{E_{\max}(s), g\cos\gamma(s)/2\mu_2(s)\}, & s \in \Gamma_2 \cup \Gamma_3, \\ E_{\max}(s), & \text{otherwise} \end{cases}$$

where

$$\Gamma_1 = \{s | \psi'(s) \neq 0, \gamma'(s) = 0, s \in [s_0, s_f]\}$$
$$\Gamma_2 = \{s | \psi'(s) \neq 0, \gamma'(s) \neq 0, \mu_1(s) \leq 0, \mu_2(s) > 0, s \in [s_0, s_f]\}$$
$$\Gamma_3 = \{s | \psi'(s) \neq 0, \gamma'(s) \neq 0, \mu_1(s) > 0, s \in [s_0, s_f]\}$$

The second constraint is defined according to the inequalities

$$\underline{g}_{w2}(s) \triangleq \max\{\underline{g}_{w1}(s), \underline{g}_{w3}(s)\} \leq E(s) \leq \bar{g}_{w2}(s), \qquad s \in [s_0, s_f] \tag{40}$$

where,

$$\underline{g}_{w3}(s) \triangleq \begin{cases} \max\{E_{\min}(s), g\cos\gamma(s)/2\mu_1(s)\}, & s \in \Gamma_3, \\ E_{\min}(s), & s \in [s_0, s_f]/\Gamma_3 \end{cases} \tag{41}$$

and

$$\bar{g}_{w2}(s) \triangleq \begin{cases} E_{\max}(s), & s \in \Gamma_3, \\ \bar{g}_{w1}(s), & s \in [s_0, s_f]/\Gamma_3 \end{cases} \tag{42}$$

and where $\mu_0(s)$, $\mu_1(s)$, and $\mu_2(s)$ are given in Eqs. (32), (34), and (35), respectively.

The collection of points $(s, E(s))$ satisfying either Eqs. (39) or (40) correspond to the set $\mathcal{W} = \mathcal{W}_1 \cup \mathcal{W}_2$ in the s-E plane, where $\mathcal{W}_1$ and $\mathcal{W}_2$ are given by

$$\mathcal{W}_i = \{(s, E) | \underline{g}_{wi}(s) \leq E \leq \bar{g}_{wi}(s), s \in [s_0, s_f]\}, \qquad i = 1, 2 \tag{43}$$

Consequently, the given geometric path is feasible only if there exists a continuous function E, whose graph lies entirely in $\mathcal{W}$, while connecting the initial and final boundary conditions. It is always assumed that $(s_0, E(s_0)) \in \mathcal{W}$ and $(s_f, E(s_f)) \in \mathcal{W}$, otherwise the problem is clearly infeasible.

It should be noted that, although only control and speed constraints are considered in this paper for the sake of brevity, addressing additional constraints is possible as long as these constraints can be converted into algebraic constraints on E. For example, it can be shown that an upper bound on the load factor $L/mg \leq n_{\max}$ is equivalent to an upper bound on E as follows:

$$E(s) \leq g\frac{-\cos\gamma(s)\gamma'(s) + \sqrt{(\cos\gamma(s)\gamma'(s))^2 + (\gamma'^2(s) + \psi'^2(s)\cos^2\gamma(s))(n_{\max}^2 - \cos^2\gamma(s))}}{2(\gamma'^2(s) + \psi'^2(s)\cos^2\gamma(s))} \tag{44}$$

The details are left to the interested reader.

D. Topological Properties of the Admissible Velocity Set

Before proceeding with the determination of the optimal velocity profile inside the admissible velocity set $\mathcal{W}$, some observations regarding the topological properties of $\mathcal{W}$ and its boundary are in order.

1) If $\mathcal{W}$ is not connected, then the given path is not feasible.

2) Even if the admissible velocity set $\mathcal{W}$ is connected, it may not be simply connected. If $\mathcal{W}$ is simply connected, then there exist two piecewise analytic functions $\underline{g}_w$ and $\bar{g}_w$ such that

$$\mathcal{W} = \{(s, E) | \underline{g}_w(s) \leq E(s) \leq \bar{g}_w(s), s \in [s_0, s_f]\} \tag{45}$$

For instance, one can simply take $\underline{g}_w = \min\{\underline{g}_{w1}, \underline{g}_{w2}\}$ and $\bar{g}_w = \max\{\bar{g}_{w1}, \bar{g}_{w2}\}$.

3) In case $\mathcal{W}$ is not simply connected, then it cannot be characterized by inequalities involving only two piecewise analytic functions as in Eq. (45). Such a situation will occur if there exist points $s \in [s_0, s_f]$ such that $\underline{g}_{w1}(s) > \bar{g}_{w2}(s)$ or $\underline{g}_{w2}(s) > \bar{g}_{w1}(s)$, for instance. Nonetheless, owing to the piecewise analyticity of the functions involved in Eq. (43), which represent the boundaries of $\mathcal{W}_1$ and $\mathcal{W}_2$ between s_0 and s_f, respectively, these functions may intersect at only at a finite number of points in $[s_0, s_f]$ [20]. Consequently, there can only be a finite number of "holes" in $\mathcal{W}$.

4) Suppose $\mathcal{W}$ is not simply connected, but it rather has m holes. In this (rather rare) case, $\mathcal{W}$ can be decomposed as the union of 2^m simply connected subsets, as illustrated in Fig. 1 for the case when $m = 1$. After such a decomposition, each subset is searched for an optimal kinetic energy profile candidate using the approach described later on in the paper. Once all possible (at most 2^m) candidates have been obtained, they are compared to identify the unique optimal kinetic energy profile for the original set $\mathcal{W}$.

This paper focuses on the simple (and most common) case when $\mathcal{W}$ is simply connected and hence $\mathcal{W}$ is defined by algebraic constraints of the form $\underline{g}_w(s) \leq E(s) \leq \bar{g}_w(s)$, $s \in [s_0, s_f]$, where $\underline{g}_w$ and $\bar{g}_w$ are appropriately defined piecewise analytic functions.

E. Thrust Constraint

From Eqs. (10), (22), and (23), the following equation is obtained:

$$\begin{aligned} T = {} & mvv' + \left(\frac{1}{2}C_{D_0}(v, s)\rho S + \frac{2K(v, s)m^2\gamma'^2}{\rho S}\right. \\ & \left. + \frac{2K(v, s)m^2\cos^2\gamma\psi'^2}{\rho S}\right)v^2 + \frac{2K(v, s)m^2g^2\cos^2\gamma}{\rho S}\frac{1}{v^2} \\ & + \frac{4K(v, s)m^2\gamma' g\cos\gamma}{\rho S} + mg\sin\gamma \end{aligned} \tag{46}$$

Note that

$$vv' = v\frac{\mathrm{d}v}{\mathrm{d}s} = \frac{\mathrm{d}}{\mathrm{d}s}\left(\frac{v^2}{2}\right) = E'$$

With a minor abuse of notation, the preceding equation can be rewritten as a constraint on the derivative of E as follows

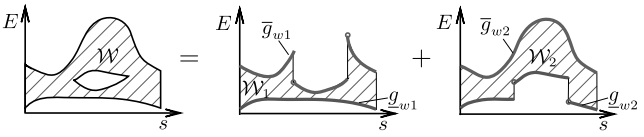

Fig. 1 Decomposition of $\mathcal{W}$ when it is not simply connected.

$$E'(s) = \frac{T(s)}{m} + c_1(E,s)E(s) + \frac{c_2(E,s)}{E(s)} + c_3(E,s) \tag{47}$$

where

$$c_1(E,s) \triangleq -\frac{C_{D_0}(E,s)\rho(s)S}{m} - \frac{4K(E,s)m\gamma'^2(s)}{\rho(s)S} - \frac{4K(E,s)m\cos^2\gamma(s)\psi'^2(s)}{\rho(s)S} \tag{48}$$

$$c_2(E,s) \triangleq -\frac{K(E,s)mg^2\cos^2\gamma(s)}{\rho(s)S} \tag{49}$$

$$c_3(E,s) \triangleq -\frac{4K(E,s)m\gamma'(s)g\ \cos\gamma(s)}{\rho(s)S} - g\ \sin\gamma(s) \tag{50}$$

It is assumed that K and C_{D_0} (hence, c_1, c_2, and c_3) are continuously differentiable with respect to E.

IV. Optimal Control Formulation

The extensive analysis of the previous section reveals that instead of working with the original dynamical system described by Eqs. (7–12), it would suffice to solve an optimal control problem with just one state variable E and one single control input T. In this section, it is proved that the thrust control switching structure is unique when the speed constraint is not active.

The optimal thrust profile $T^*(s)$ and the corresponding optimal speed $v^*(s) = \sqrt{2E^*(s)}$ for the minimum-time travel of a fixed-wing aircraft are given by the solution to the following optimal control problem:

Problem 4.1 (Time Path-Tracking Problem): Consider the following optimal control problem in Lagrange form:

$$\min_T J(s_0, s_f, E(s_0), E(s_f), T) = t_f = \int_{s_0}^{s_f} \frac{\mathrm{d}s}{\sqrt{2E(s)}} \tag{51a}$$

$$\text{subject to } E'(s) = \frac{T(s)}{m} + c_1(E,s)E(s) + \frac{c_2(E,s)}{E(s)} + c_3(E,s) \tag{51b}$$

$$\underline{g}_w(s) \le E(s) \le \bar{g}_w(s) \tag{51c}$$

$$E(s_0) = v_0^2/2 \tag{51d}$$

$$E(s_f) = v_f^2/2 \tag{51e}$$

$$T_{\min} \le T(s) \le T_{\max} \tag{51f}$$

where v_0 and v_f are the required initial and final speed at s_0 and s_f, respectively, and $\bar{g}_w$ and $\underline{g}_w$ are piecewise analytic functions, computed in Sec. III.

Note that the value of $\bar{g}_w$ and $\underline{g}_w$ can always be redefined at their (necessarily finite) points of discontinuities to make them either left or right continuous. In particular, and without loss of generality, in this paper, it is assumed that, at the point of discontinuity, the value of $\bar{g}_w$ is defined so that it is lower semicontinuous, and the value of $\underline{g}_w$ is defined so that it is upper semicontinuous.[§] The reasons for such an assumption will be explained in Sec. V. The functions c_1, c_2, and c_3 are also piecewise analytic, and are given in Eqs. (48–50). They can be readily computed once the path is given.

Consider the case when the state constraint (51c) is not active. The Hamiltonian of the optimal control problem is

$$H(E,\lambda,T,s) = \frac{1}{\sqrt{2E}} + \lambda\left(\frac{T}{m} + c_1(E,s)E + \frac{c_2(E,s)}{E} + c_3(E,s)\right)$$

The costate dynamics is

$$\lambda' = -\frac{\partial H(E,\lambda,T,s)}{\partial E} = \frac{1}{2\sqrt{2}}E^{-3/2} - \lambda\left(c_1(E,s) - c_2(E,s)E^{-2} + \frac{\partial c_1(E,s)}{\partial E}E + \frac{\partial c_2(E,s)}{\partial E}\frac{1}{E} + \frac{\partial c_3(E,s)}{\partial E}\right) \tag{52}$$

The optimal control consists of constrained [i.e., $E(s) = \underline{g}_w(s)$ or $E(s) = \bar{g}_w(s)$] and unconstrained [i.e., $\underline{g}_w(s) < E(s) < \bar{g}_w(s)$] arcs. Furthermore, the control T enters linearly into the Hamiltonian, and so a singular control may exist. The switching function is

$$\frac{\partial H}{\partial T} = \frac{\lambda}{m} \tag{53}$$

According to Pontryagin's maximum principle, depending on the sign of the switching function, the optimal control may switch between the two bounds $T_{\min}, T_{\max}$ and the singular control when the state constraints are not active. Correspondingly, in general, the optimal control T^* of Problem 4.1 may contain bang–bang control, singular control, and control arcs associated with active state constraints, as described by the following expression:

$$T^*(s) = \begin{cases} T_{\min}, & \text{for } \lambda > 0, s \in [s_0, s_f] \setminus \mathcal{K}, \\ \text{singular control} & \text{for } \lambda = 0, s \in [s_0, s_f] \setminus \mathcal{K}, \\ T_{\max}, & \text{for } \lambda < 0, s \in [s_0, s_f] \setminus \mathcal{K}, \\ \bar{T}_w(s), & \text{for } s \in \mathcal{K}_U, \\ \underline{T}_w(s), & \text{for } s \in \mathcal{K}_L \end{cases} \tag{54}$$

where $\mathcal{K}_U = \{s | E^*(s) = \bar{g}_w(s), s \in [s_0, s_f]\}$, $\mathcal{K}_L = \{s | E^*(s) = \underline{g}_w(s), s \in [s_0, s_f]\}$, and $\mathcal{K} = \mathcal{K}_U \cup \mathcal{K}_L$. At the points where the function $\bar{g}_w$ (respectively, $\underline{g}_w$) is differentiable, the value of the thrust $\bar{T}_w(s)$ (respectively, $\underline{T}_w$) is computed by

$$\bar{T}_w(s) = m(\bar{g}'_w(s) - c_1(\bar{g}_w(s), s)\bar{g}_w(s) - c_3(\bar{g}_w(s), s) - c_2(\bar{g}_w(s), s)/\bar{g}_w(s)) \tag{55}$$

And, respectively,

$$\underline{T}_w(s) = m(\underline{g}'_w(s) - c_1(\underline{g}_w(s), s)\underline{g}_w(s) - c_3(\underline{g}_w(s), s) - c_2(\underline{g}_w(s), s)/\underline{g}_w(s)) \tag{56}$$

At the points where $\bar{g}_w$ (respectively, $\underline{g}_w$) is discontinuous and/or nondifferentiable, the thrust is discontinuous and can be computed by

$$\bar{T}_w(s^\pm) = m(\bar{g}'_w(s^\pm) - c_1(\bar{g}_w(s^\pm), s)\bar{g}_w(s^\pm) - c_3(\bar{g}_w(s^\pm), s) - c_2(\bar{g}_w(s^\pm), s)/\bar{g}_w(s^\pm)) \tag{57}$$

and

[§]It is reminded that the function $f\colon [t_0, t_f] \mapsto \mathbb{R}$ is *upper semi-continuous* (respectively, *lower semi-continuous*) at $t \in [t_0, t_f]$ if $\lim\sup_{\tau\to t} f(\tau) \le f(t)$ (resp. $\lim\inf_{\tau\to t} f(\tau) \ge f(t)$), and, in addition, $\lim\sup_{\tau\downarrow t_0} f(\tau) \le f(t_0)$ (resp. $\lim\inf_{\tau\downarrow t_0} f(\tau) \ge f(t_0)$) and $\lim\sup_{\tau\uparrow t_f} f(\tau) \le f(t_f)$ (resp. $\lim\inf_{\tau\uparrow t_f} f(\tau) \ge f(t_f)$).

$$\underline{T}_w(s^{\pm}) = m(\underline{g}_w'(s^{\pm}) - c_1(\underline{g}_w(s^{\pm}), s)\underline{g}_w(s^{\pm}) - c_3(\underline{g}_w(s^{\pm}), s) - c_2(\underline{g}_w(s^{\pm}), s)/\underline{g}_w(s^{\pm})) \tag{58}$$

for the two cases. Note that, owing to the piecewise continuous differentiability of $\bar{g}_w$ and $\underline{g}_w$, the limits $\bar{g}_w'(s^{\pm})$, $\bar{g}_w(s^{\pm})$ and $\underline{g}_w'(s^{\pm})$, $\underline{g}_w(s^{\pm})$ exist for all $s \in [s_0, s_f]$. Furthermore, the number of points at which $\bar{g}_w'(s^+) \neq \bar{g}_w'(s^-)$, or $\underline{g}_w'(s^+) \neq \underline{g}_w'(s^-)$, or $\bar{g}_w(s^+) \neq \bar{g}_w(s^-)$, or $\underline{g}_w(s^+) \neq \underline{g}_w(s^-)$ is finite.

Proposition 4.1: The optimal control solution of Problem 4.1 does not contain any singular control.

Proof: It is sufficient to show that there does not exist any subinterval $[s_a, s_b] \subseteq [s_0, s_f]$ on which $\lambda(s) \equiv 0$ and $\underline{g}_w(s) < E(s) < \bar{g}_w(s)$ (strict inequalities) for all $s \in [s_a, s_b]$. Suppose, ad absurdum, that $\lambda(s) \equiv \lambda'(s) \equiv 0$ for all $s \in [s_a, s_b]$, and the state constraints are not active on $[s_a, s_b]$. It follows that, on $[s_a, s_b]$, Eq. (52) becomes

$$0 = \frac{1}{2\sqrt{2}} E^{-3/2} > 0$$

which is impossible. Hence, λ cannot remain constantly zero on any nontrivial interval, and the proof is complete. □

Proposition 4.2: The optimal control $T^*(s)$ is bang–bang and does not contain any switch from $T_{\min}$ to $T_{\max}$ on $[s_0, s_f] \setminus \mathcal{K}$.

Proof: Because it has been shown that a singular control does not exist, the control history must be bang–bang on $[s_0, s_f] \setminus \mathcal{K}$. It is sufficient to prove that, when the constraint (51c) is inactive, there does not exist a switching from $T_{\min}$ to $T_{\max}$ in the optimal control history.

To this end, suppose, on the contrary, that T^* contains a switching from $T_{\min}$ to $T_{\max}$ at some $s_m \in (s_a, s_b] \subset ([s_0, s_f] \setminus \mathcal{K})$, such that

$$T^* = \begin{cases} T_{\min}, & s_a < s \le s_m, \\ T_{\max}, & s_m < s \le s_b \end{cases}$$

For simplicity, and without loss of generality, it is assumed that the functions c_1, c_2, and c_3 are continuous at s_m.

Let η be a small positive scalar, and let $E_m^-(s;\eta)$ and $E_m^+(s;\eta)$ denote the trajectories passing through $(s_m, E^*(s_m) + \eta)$, with control $T_{\min}$ and $T_{\max}$, respectively. From the definitions of $E_m^-(s;\eta)$ and $E_m^+(s;\eta)$, the following expression holds:

$$\begin{aligned} E_m^{-\prime}(s;\eta) - E_m^{+\prime}(s;0) &= (T_{\min} - T_{\max})/m \\ &+ c_1(E_m^-(s;\eta), s)E_m^-(s;\eta) - c_1(E_m^+(s;0), s)E_m^+(s;0) \\ &+ \frac{c_2(E_m^-(s;\eta), s)E_m^+(s;0) - c_2(E_m^+(s;0), s)E_m^-(s;\eta)}{E_m^-(s;\eta)E_m^+(s;0)} \\ &+ c_3(E_m^-(s;\eta), s) - c_3(E_m^+(s;0), s) \end{aligned} \tag{59}$$

In the right-hand-side of Eq. (59), the absolute value of terms containing c_1 is

$$\begin{aligned} &|c_1(E_m^-(s;\eta), s)E_m^-(s;\eta) - c_1(E_m^+(s;0), s)E_m^+(s;0)| \\ &\quad = |c_1(E_m^-(s;\eta), s)(E_m^-(s;\eta) - E_m^+(s;0)) \\ &\quad + (c_1(E_m^-(s;\eta), s) - c_1(E_m^-(s;0), s))E_m^+(s;0) \\ &\quad + (c_1(E_m^-(s;0), s) - c_1(E_m^+(s;0), s))E_m^+(s;0)| \\ &\quad = |c_1(E_m^-(s;\eta), s)(E_m^-(s;\eta) - E_m^+(s;0)) \\ &\quad + (c_1(E_m^-(s;\eta), s) - c_1(E_m^-(s;0), s))E_m^+(s;0)| \\ &\quad \le |c_1(E_m^-(s;\eta), s)||(E_m^-(s;\eta) - E_m^+(s;0))| \\ &\quad + |(c_1(E_m^-(s;\eta), s) - c_1(E_m^-(s;0), s))||E_m^+(s;0)| \end{aligned} \tag{60}$$

where the fact that $E_m^-(s;0) = E_m^+(s;0)$ is used. Note that $E_m^+(s_m;\eta) = E_m^-(s_m;\eta) = E^*(s_m) + \eta$. Thus,

$$\begin{aligned} |E_m^-(s;\eta) - E_m^+(s;0)| &= |E_m^-(s;\eta) - E_m^-(s_m;\eta) + E_m^+(s_m;\eta) \\ &\quad - E_m^+(s_m;0) + E_m^+(s_m;0) - E_m^+(s;0)| \\ &\le |E_m^-(s;\eta) - E_m^-(s_m;\eta)| + |E_m^+(s_m;\eta) - E_m^+(s_m;0)| \\ &\quad + |E_m^+(s_m;0) - E_m^+(s;0)| \end{aligned}$$

Because $E_m^-(s;\eta)$ and $E_m^+(s;0)$ are continuous with respect to s, and $E_m^+(s_m;\eta)$ is continuous with respect to η, $|E_m^-(s;\eta) - E_m^+(s;0)|$ can be arbitrarily small by decreasing η and $|s - s_m|$. Therefore, $|c_1(E_m^-(s;\eta), s)E_m^-(s;\eta) - c_1(E_m^+(s;0), s)E_m^+(s;0)|$ in Eq. (60) can be made arbitrarily small, following the continuity of c_1 and the boundedness of c_1 and $E_m^+(s;0)$. Likewise, the terms $|c_1(E_m^-(s;\eta), s) - c_1(E_m^-(s;0), s)|$, $|c_3(E_m^-(s;\eta), s) - c_3(E_m^+(s;0), s)|$, and $|c_2(E_m^-(s;\eta), s)E_m^+(s;0) - c_2(E_m^+(s;0), s)E_m^-(s;\eta)|$ in Eq. (59) can also be made arbitrarily small following the continuity of c_1, c_2, and c_3. Hence, for any $\delta > 0$, there exists $\eta_a > 0, \epsilon_a > 0$ such that $E_m^{-\prime}(s;\eta) - E_m^{+\prime}(s;0) < (T_{\min} - T_{\max})/m + \delta$ for all $\eta < \eta_a$ and $s_m - \epsilon_a < s < s_m + \epsilon_a$. Without loss of generality, let $\delta = (T_{\max} - T_{\min})/2m$, then the preceding inequality is simplified to

$$E_m^{-\prime}(s;\eta) - E_m^{+\prime}(s;0) < (T_{\min} - T_{\max})/2m \tag{61}$$

By the same token, there exists $\eta_b > 0$, $\epsilon_b > 0$, such that

$$E_m^{-\prime}(s;0) - E_m^{+\prime}(s;\eta) < (T_{\min} - T_{\max})/2m \tag{62}$$

for $\eta < \eta_b$ and $s_m - \epsilon_b < s < s_m + \epsilon_b$. Let $\varepsilon = \min\{\epsilon_a, \epsilon_b\}$ and $\eta_0 = \min\{\eta_a, \eta_b\}$ such that, for all $\eta < \eta_0$ and all $s \in (s_m - \epsilon, s_m + \epsilon)$, both Eqs. (61) and (62) are satisfied and, in particular, $E_m^{-\prime}(s;\eta) - E_m^{+\prime}(s;0) < (T_{\min} - T_{\max})/2m < 0$ and $E_m^{-\prime}(s;0) - E_m^{+\prime}(s;\eta) < (T_{\min} - T_{\max})/2m < 0$ for all $s \in (s_m - \epsilon, s_m + \epsilon)$ and $0 < \eta < \eta_0$.

Notice that, in the interval $(s_m - \epsilon, s_m + \epsilon)$, the optimal specific kinetic energy profile can be written equivalently as

$$E^*(s) = \begin{cases} E_m^-(s;0), & s_m - \epsilon < s < s_m, \\ E_m^+(s;0), & s_m < s < s_m + \epsilon \end{cases}$$

Consider now the part of $E_m^+(s;\eta)$ with $s < s_m$ and the part of $E_m^-(s;\eta)$ with $s > s_m$. Since $E^*(s_m) < \liminf_{s \to s_m} \bar{g}_w(s)$, and because $\bar{g}_w(s)$ is lower semicontinuous, there exists a small positive real number η_1 such that, for all $\eta < \eta_1$, $E_m^+(s;\eta) < \bar{g}_w(s)$ for all $s_m - \epsilon < s \le s_m$, and $E_m^-(s;\eta) < \bar{g}_w(s)$ for all $s_m < s \le s_m + \epsilon$, that is, a sufficiently small change of the initial condition at s_m will not lead to the violation of the constraint $\bar{g}_w(s)$.

Let $\eta_2 = -\epsilon(T_{\min} - T_{\max})/2m > 0$, and let $0 < \eta < \min\{\eta_0, \eta_1, \eta_2\}$. At the point s_m, $E_m^-(s_m;\eta) - E^*(s_m) = E_m^-(s_m;\eta) - E_m^-(s_m;0) = E_m^-(s_m;\eta) - E_m^+(s_m;0) = \eta > 0$. Since $E_m^{-\prime}(s;\eta) - E_m^{+\prime}(s;0) < (T_{\min} - T_{\max})/2m$ for all $s \in (s_m, s_m + \epsilon)$, forward integration of $E_m^{-\prime}(s;\eta) - E_m^{+\prime}(s;0)$ from s_m results in $E_m^-(s;\eta) - E_m^+(s;0) < \eta + (T_{\min} - T_{\max})(s - s_m)/2m$ for all $s \in (s_m, s_m + \epsilon)$, and $E_m^-(s + \epsilon;\eta) - E_m^+(s + \epsilon;0) < 0$. Therefore, by the continuity of $E_m^-(s;\eta) - E_m^+(s;0)$, there exists $s_m^+ \in (s_m, s_m + \epsilon)$ such that $E_m^-(s_m^+;\eta) = E_m^+(s_m^+;0) = E^*(s_m^+)$.

A similar argument shows that there exists $s_m^- \in (s_m - \epsilon, s_m)$ such that $E_m^+(s_m^-;\eta) = E^*(s_m^-)$. See Fig. 2.

Now consider the variation of T^* (see Fig. 3) given by

$$\delta T = \begin{cases} T_{\max} - T_{\min}, & s_m^- < s \le s_m, \\ T_{\min} - T_{\max}, & s_m < s \le s_m^+, \\ 0, & \text{otherwise} \end{cases}$$

Then with the new control $\tilde{T} = T^* + \delta T$, the new speed profile $\tilde{E}$ is composed of segments of E^*, $E_m^+(s;\eta)$ and $E_m^-(s;\eta)$, which is given next

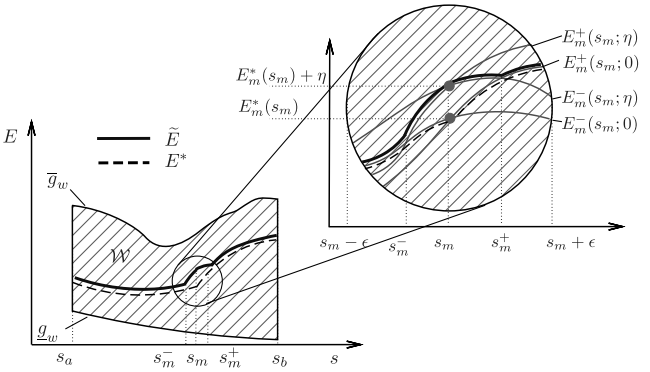

Fig. 2 Speed variation for the proof of Proposition 4.2.

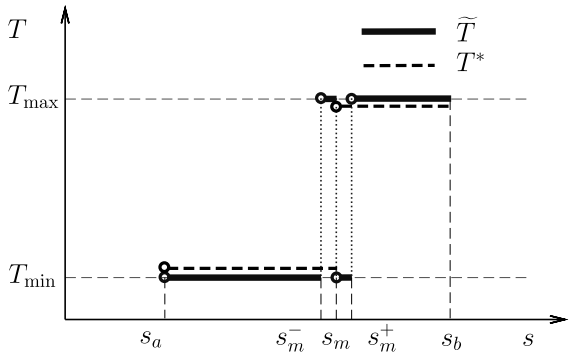

Fig. 3 Thrust variation for proof of Proposition 4.2.

$$\tilde{E}(s)=\begin{cases}E^*(s), & s_a<s\le s_m^-,\\ E_m^+(s;\eta), & s_m^-<s\le s_m,\\ E_m^-(s;\eta), & s_m<s\le s_m^+,\\ E^*(s), & s_m^+<s\le s_b\end{cases}$$

The variation of the speed is shown in Fig. 2. By construction of s_m^- and s_m^+, $E^*(s)<\tilde{E}(s)<\bar{g}_w(s)$ for $s\in(s_m^-,s_m^+)$. Hence, $J(s_a,s_b,E(s_a),E(s_b),T^*)>J(s_b,s_b,E(s_a),E(s_b),\tilde{T})$, which means that T^* cannot be optimal. □

The next proposition shows that the lower bound $\underline{g}_w$ is generically not part of the optimal specific kinetic energy profile on a nontrivial interval.

Proposition 4.3: Assume $\bar{g}_w(s)\neq\underline{g}_w(s)$ and $T^*(s)=\underline{T}_w(s)<T_{\max}(s)$ for all $s\in[s_0,s_f]$. Let $E^*(s)$ be the optimal kinetic energy solution to Problem 4.1. Then the set $\mathcal{K}_L$ does not contain any nontrivial interval.

Proof: (Sketch) Assume, on the contrary, that there exists $(s_a,s_b)\in\mathcal{K}_L$ such that $E^*(s)=\underline{g}_w(s)$ for all $s\in(s_a,s_b)$, where $s_a\neq s_b$. Then, since $\bar{g}_w(s)\neq\underline{g}_w(s)$ and $\underline{T}_w(s)<T_{\max}(s)$ on (s_a,s_b), one can construct a variation of the thrust T in the interval (s_a,s_b) similar to the proof of Proposition 4.2 that does not violate the thrust constraint, and which results in better time optimality, hence leading to a contradiction. The details of the proof are left to the interested reader. □

Corollary 4.1: The time-optimal control T^* for Problem 4.1 can be constructed as a combination of $T_{\max}$, $T_{\min}$, and $\bar{T}_w$.

Proof: Note that $T^*(s)$ is equal to $T_{\max}$, or $T_{\min}$, or $\bar{T}_w(s)$ on $[s_0,s_f]\setminus\mathcal{K}_L$. It would suffice to consider the value of $T^*(s)$ on $\mathcal{K}_L$. If $\bar{g}_w(s)=\underline{g}_w(s)$ on some nontrivial interval $[s_a,s_b]$, then clearly $T^*(s)=\underline{T}_w(s)=\bar{T}_w(s)$ for all $s\in[s_a,s_b]$, and the corollary holds on $[s_a,s_b]$. If $\underline{T}_w(s)=T_{\min}(s)$ for some $s\in[s_0,s_f]$, then the corollary trivially holds for such points. If $\bar{g}_w(s)=\underline{g}_w(s)$ only at isolated points, or if $\bar{g}_w(s)\neq\underline{g}_w(s)$ and $\underline{T}_w(s)<T_{\max}(s)$ for all $s\in[s_0,s_f]$, then $\mathcal{K}_L$ has an empty interior according to Proposition 4.3. □

V. Two Numerical Algorithms for Finding the Optimal Control

Recall that the admissible kinetic energy set $\mathcal{W}$ is determined by the geometry of the given path. Once the path is given, it is possible to find a semi-analytical solution of the optimal control problem (51a) using the necessary conditions introduced in the previous section. Assuming that the given path is feasible, then, according to Proposition 4.3, the lower bound $\underline{g}_w$ cannot be part of the optimal kinetic energy profile, except for the trivial case when $\underline{g}_w(s)=\bar{g}_w(s)$ over some part of $[s_0,s_f]$. The optimal kinetic energy profile is thus composed of three types of segments corresponding to maximum acceleration with $T^*=T_{\max}$, maximum deceleration with $T^*=T_{\min}$, and $T^*=\bar{T}_w$, the latter corresponding to the saturation of the upper state constraint $E(s)=\bar{g}_w(s)$. The most critical step of the optimal synthesis problem is to characterize which parts of $\bar{g}_w$ can possibly be saturated.

If $\bar{g}_w$ is continuous at $s_d\in[s_0,s_f]$ and $E^*(s_d)=\bar{g}_w(s_d)$, because $E^*(s)$ cannot violate the constraint $\bar{g}_w$ [i.e., $E^*(s)\le\bar{g}_w(s)$], there exists a control $T^*(s)\in[T_{\min},T_{\max}]$ such that $E^*(s)$ satisfies the following inequality:

$$\frac{E^*(s_d+h)-E^*(s_d)}{h}\le\frac{\bar{g}_w(s_d+h)-\bar{g}_w(s_d)}{h}\tag{63}$$

where h is a small positive real number. By taking the limits of both sides of inequality (63) with $h\to0$, the last expression leads to the existence of $T^*(s)\in[T_{\min},T_{\max}]$, such that

$$E^{*\prime}(s_d^+)\le\bar{g}_w'(s_d^+)\tag{64}$$

On the other hand,

$$\begin{aligned}E^{*\prime}(s_d^+)\in\Bigg[&\frac{T_{\min}}{m}+c_1(E^*(s_d),s_d^+)E^*(s_d)+\frac{c_2(E^*(s_d),s_d^+)}{E^*(s_d)}\\&+c_3(E^*(s_d),s_d^+),\frac{T_{\max}}{m}+c_1(E^*(s_d),s_d^+)E^*(s_d)\\&+\frac{c_2(E^*(s_d),s_d^+)}{E^*(s_d)}+c_3(E^*(s_d),s_d^+)\Bigg]\end{aligned}$$

Therefore, inequality (64) implies

$$\begin{aligned}\bar{g}_w'(s_d^+)\ge&\frac{T_{\min}}{m}+c_1(E^*(s_d),s_d^+)E^*(s_d)+\frac{c_2(E^*(s_d),s_d^+)}{E^*(s_d)}\\&+c_3(E^*(s_d),s_d^+)=\frac{T_{\min}}{m}+c_1(\bar{g}_w(s_d),s_d^+)\bar{g}_w(s_d)\\&+\frac{c_2(\bar{g}_w(s_d),s_d^+)}{\bar{g}_w(s_d)}+c_3(\bar{g}_w(s_d),s_d^+)\end{aligned}\tag{65}$$

Similarly, the constraint $E^*(s)\le\bar{g}_w(s)$ for $s\in(s_d-\epsilon,s_d]$ implies

$$\begin{aligned}\bar{g}_w'(s_d^-)\le&\frac{T_{\max}}{m}+c_1(E^*(s_d),s_d^-)E^*(s_d)+\frac{c_2(E^*(s_d),s_d^-)}{E^*(s_d)}\\&+c_3(E^*(s_d),s_d^-)=\frac{T_{\max}}{m}+c_1(\bar{g}_w(s_d),s_d^-)\bar{g}_w(s_d)\\&+\frac{c_2(\bar{g}_w(s_d),s_d^-)}{\bar{g}_w(s_d)}+c_3(\bar{g}_w(s_d),s_d^-)\end{aligned}\tag{66}$$

Therefore, $E^*(s_d)=\bar{g}_w(s_d)$ is possible only if both inequalities (65) and (66) are satisfied. In particular, when $\bar{g}_w$ is continuously differentiable at s_d, then $\bar{g}_w'(s_d^-)=\bar{g}_w'(s_d^+)=\bar{g}_w'(s_d)$ and, hence, the inequalities (65) and (66) are reduced to

$$\frac{T_{\min}}{m} + c_1(\bar{g}_w(s_d), s_d^+)\bar{g}_w(s_d) + \frac{c_2(\bar{g}_w(s_d), s_d^+)}{\bar{g}_w(s_d)} + c_3(\bar{g}_w(s_d), s_d^+) \le \bar{g}'_w(s_d) \le \frac{T_{\max}}{m} + c_1(\bar{g}_w(s_d), s_d^-)\bar{g}_w(s_d) + \frac{c_2(\bar{g}_w(s_d), s_d^-)}{\bar{g}_w(s_d)} + c_3(\bar{g}_w(s_d), s_d^-) \tag{67}$$

If $\bar{g}_w$ is discontinuous at s_d, then either $\bar{g}_w(s_d) = \bar{g}_w(s_d^+)$ or $\bar{g}_w(s_d) = \bar{g}_w(s_d^-)$. In this case, the conditions $E^*(s_d) = \bar{g}_w(s_d)$ and $E^*(s) \le \bar{g}_w(s)$ in a neighborhood of s_d can be satisfied only if $\bar{g}_w(s)$ is lower semicontinuous (which is assumed) and, in addition, inequality (65) holds if $\bar{g}_w(s_d^+) < \bar{g}_w(s_d^-)$, and inequality (66) holds if $\bar{g}_w(s_d^+) > \bar{g}_w(s_d^-)$.

Let $\bar{W}$ be the graph of all points in the interval $[s_0, s_f]$ such that $\bar{g}_w$ is continuous, and, in addition, inequalities (65) and (66) hold, that is,

$$\tilde{W} \triangleq \{(s_d, \bar{g}_w(s_d))|\ (65) \text{ and } (66) \text{ hold}, s_d \in [s_0, s_f]\}$$

These are the points on the graph of $\bar{g}_w(s)$, which could possibly be part of the optimal kinetic energy profile $E^*(s)$. Furthermore, let $\tilde{W}_d$ be the points on the graph of $\bar{g}_w$ where $\bar{g}_w$ is discontinuous (but necessarily lower semicontinuous), and either inequality (65) or (66) holds. The points in $\tilde{W}_d$ are the points of discontinuity of $\bar{g}_w$ which could be part of the optimal $E^*(s)$ profile.

Let $\bar{W} = \tilde{W} \bigcup \tilde{W}_d$ and let $\bar{W}^c = \{(s, \bar{g}_w(s)), s \in [s_0, s_f]\} \setminus \bar{W}$. Generally, $\bar{W}$ is disconnected. Depending on the path, $\bar{W}$ may consist of multiple arcs and single points, as shown in Fig. 4. By the piecewise analyticity assumption of the given path, all functions involved in inequalities (65) and (66) are piecewise analytic, and it follows that the equality in (65) and (66) can only hold for a finite number of points on $[s_0, s_f]$. Hence, $\bar{W}$ is composed of only a finite union of disjoint components. That is, $\bar{W} = \bigcup_{j=1}^{N-1} \bar{W}_j$ for some positive integer N, where $\bar{W}_j$ are connected, and with $\bar{W}_i \bigcap \bar{W}_j = \varnothing$ for $i \neq j$. Let (s_j^-, E_j^-) and (s_j^+, E_j^+) denote the left- and right-end points of $\bar{W}_j$ for each $j = 1, \ldots, N-1$, where $E_j^- = \bar{g}_w(s_j^-)$ and $E_j^+ = \bar{g}_w(s_j^+)$ correspond to the "trajectory sink" and the "trajectory source" in [16]. Also, define two points $\bar{W}_0 = (s_0, E_0)$ and $\bar{W}_N = (s_f, E_f)$. Note that, in general, $\bar{W}_0 \neq \bar{W}_1$ and $\bar{W}_N \neq \bar{W}_{N-1}$. It is obvious that $\bar{W}_0$ and $\bar{W}_N$ must be part of the graph of the optimal kinetic energy profile.

For each $j = 1, \ldots, N-1$, let $\mathcal{S}_j^+$ denote the trajectory obtained by forward integration with maximum thrust, starting from s_j^+ with the initial value $\mathcal{S}_j^+(s_j^+) \triangleq E_j^+$, and, similarly, let $\mathcal{S}_j^-$ be the trajectory obtained by backward integration using minimum thrust, starting from s_j^- with the initial value $\mathcal{S}_j^-(s_j^-) \triangleq E_j^-$. Forward integration with $T_{\max}$ and backward integration with $T_{\min}$ are also computed from the boundary points s_0 and s_f with initial conditions E_0 and E_f, respectively, and the resulting trajectories are denoted with $\mathcal{S}_0^+$ and $\mathcal{S}_N^-$.

All current algorithms, including those in [13–16], use a "search, integrate, and check" procedure, which gradually extend the optimal speed profile from the initial point to the final point. Following the same procedure, it is possible that, during the search process, part of the already constructed trajectory has to be discarded because it cannot intersect $\bar{W}$ later on for any allowable thrust value.

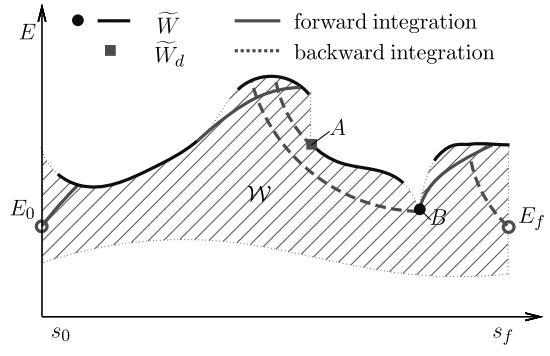

Fig. 4 Elements for the optimal E.

To avoid such unnecessary computations, and to also improve the overall computational efficiency of the numerical scheme, it is necessary to characterize the elements in $\bar{W}$ that are part of E^*. Assuming feasibility of the problem, when the boundary conditions cannot be satisfied by a bang–bang control with no more than one switch from $T_{\max}$ to $T_{\min}$, some elements in $\bar{W}$ corresponding to the smaller values of $\bar{g}_w(s)$ must be active (at least at a single point) in the optimal solution because these correspond to the most stringent/binding part of the constraint. Following this observation, two new algorithms are introduced with improved numerical efficiency for searching the optimal speed profile. The first algorithm is designed for parallel computation, whereas the second algorithm reduces the amount of computations devoted to the search, integrate, and check process.

A. Algorithm 1

Step 1) Compute $\bar{g}_w$, $\underline{g}_w$ as in Sec. III.C and check the feasibility of the geometric path. Stop if the path is not feasible, otherwise proceed to the next step.

Step 2) Compute the feasible segments $\bar{W}_j$ on the graph of $\bar{g}_w$ following the procedure outlined in the previous section.

Step 3) Calculate $\mathcal{S}_j^+$ for $j = 0, 1, 2, \ldots, N-1$, with the integration terminated when $\bar{g}_w(s) = \mathcal{S}_j^+(s)$, or $s = s_f$. Let I_j^+ denote the interval of integration associated with $\mathcal{S}_j^+$. Also calculate $\mathcal{S}_j^-$ for $j = 1, 2, \ldots, N$, with the integration terminated when $\bar{g}_w(s) = \mathcal{S}_j^-(s)$, or $s = s_0$ and denote by I_j^- the corresponding intervals of integration of $\mathcal{S}_j^-$.

Step 4) Let

$$S^{\pm}(s) = \begin{cases} \mathcal{S}^{\pm}(s), & s \in I_j^{\pm}, \\ \bar{g}_w(s), & s \in [s_0, s_f] \setminus I_j^{\pm} \end{cases} \tag{68}$$

for all $j = 0, 1, \ldots, N$, and let

$$E(s) \triangleq \min\{S_0^+(s), S_1^+(s), \ldots, S_{N-1}^+(s), S_1^-(s), S_2^-(s), \ldots, S_N^-(s)\} \tag{69}$$

If $E(0) = E_0$, $E(s_f) = E_f$, and $E(s) \ge \underline{g}_w(s)$ for all $s \in [s_0, s_f]$, then the optimal speed profile is given by Eq. (69). Otherwise the given path is not feasible.

The optimal speed profile is given by $v^*(s) = \sqrt{2E^*(s)}$, and the corresponding optimal thrust profile $T^*(s)$ can be computed by Eq. (46). By construction, the optimal thrust profile $T^*(s)$ satisfies the necessary conditions given by Proposition 4.2 and Corollary 4.1. The control T^* is indeed optimal because it maximizes pointwise the speed, and any further increase in speed results in the violation of the speed constraint.

Note that the search, integrate, and check process is avoided in this algorithm. This algorithm can be implemented in parallel owing to the following reasons: 1) Steps 1 and 4 can be performed pointwise for different $s \in [s_0, s_f]$; 2) in steps 2 and 3, the computations of $\mathcal{S}_j^-$ and $\mathcal{S}_j^+$ are independent, hence they can be computed in parallel for different j at the same time.

The following algorithm still preserves the search, integrate, and check process, but the repetition of the process is reduced to a minimum.

B. Algorithm 2

Step 1) Compute $\bar{g}_w$, $\underline{g}_w$, and check the feasibility of the geometric path. Stop if the path is not feasible, otherwise proceed to the next step.

Step 2) Compute $\mathcal{S}_0^+(s)$ and $\mathcal{S}_N^-(s)$ with stopping criteria $\mathcal{S}_0^+(s) = \bar{g}_w(s)$ and $\mathcal{S}_N^-(s) = \bar{g}_w(s)$, or $s = s_0$, or $s = s_f$. Update $\bar{g}_w(s) \leftarrow \mathcal{S}_0^+(s)$ and $\bar{g}_w(s) \leftarrow \mathcal{S}_N^-(s)$ on the corresponding domain of integration.

Step 3) Compute $\bar{W}$ and its segments $\bar{W}_j$ on the graph of $\bar{g}_w$ following the procedure outlined previously. If $\bar{g}_w$ is continuous

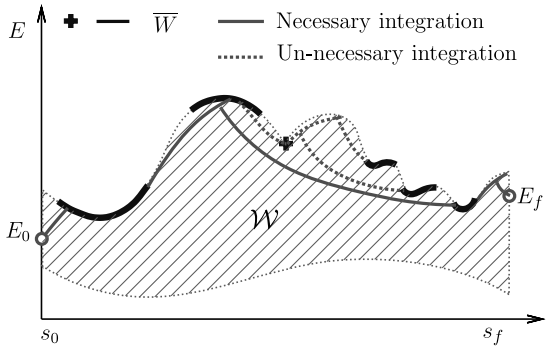

Fig. 5 Algorithm comparison.

and $\bar{W}^c$ is empty, or if $\bar{g}_w(s_0) \neq E(s_0)$, or if $\bar{g}_w(s_f) \neq E(s_f)$, then go to step 5. Otherwise, go to the next step.

Step 4) Among those $\bar{W}_j$ for which no integration has been performed at s_j^+ and s_j^-, select the one whose distance to the s axis is the smallest. Let its index be k. Compute $\mathcal{S}_k^-(s)$ and $\mathcal{S}_k^+(s)$ with the stopping criteria $\mathcal{S}_k^-(s) = \bar{g}_w(s)$ and $\mathcal{S}_k^+(s) = \bar{g}_w(s)$, or $s = 0$, or $s = s_f$. Update $\bar{g}_w(s) \leftarrow \mathcal{S}_k^-(s)$ and $\bar{g}_w(s) \leftarrow \mathcal{S}_k^+(s)$ on the corresponding domain of integration, and go to step 3.

Step 5) If $\bar{g}_w(s_0) \neq E(s_0)$ or $\bar{g}_w(s_f) \neq E(s_f)$, then the given path is infeasible. Otherwise, the optimal speed profile is given by $E^* = \bar{g}_w$.

The difference between Algorithm 1 and Algorithm 2 (as well as the other time-optimal control algorithms in [13–16]) is illustrated in Fig. 5. Although Algorithm 2 computes only the integrations that are involved in the construction of the optimal speed profile, the algorithms in [13–16] integrate the trajectory along arcs that may be discarded later on when extending the optimal speed profile to the final point. Hence, they are in general less efficient when compared with Algorithm 2.

VI. Numerical Examples

In this section, two examples are used to test the feasibility and optimality of the proposed approach. Both examples implement Algorithm 1, for simplicity. The first example focuses on checking the feasibility of the algorithm (i.e., whether the controls given by the optimal parameterization method satisfy the prescribed bounds) and whether the aircraft can follow the given path when using these control inputs. In the second example, the given path is a minimum-time path with known time-parameterization, and it is used to confirm the optimality of the proposed method.

A. Landing Path with Two Turns

A three-dimensional path is used to test the feasibility of the trajectories obtained using the proposed time-parameterization method. The trajectory is shown in Figs. 6 and 7. The initial position of the aircraft is (0,0,6) km, the aircraft flies with $\nu_0 = 220\ m/s$ at

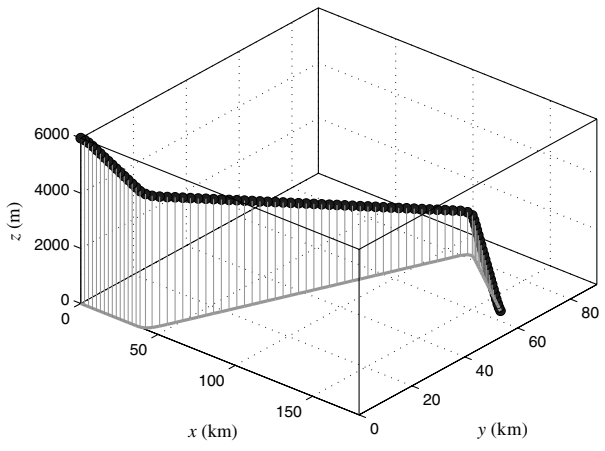

Fig. 6 Three-dimensional geometric trajectory.

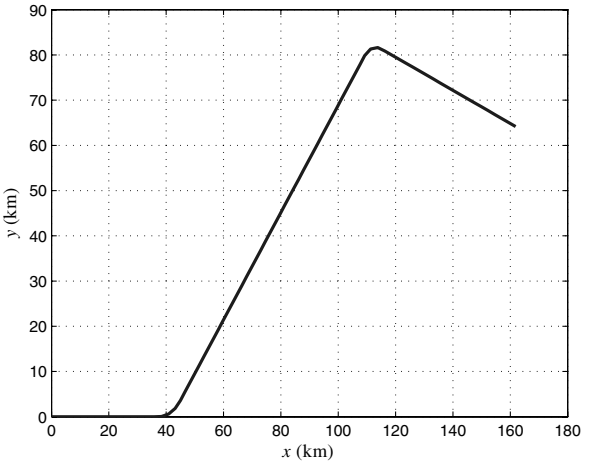

Fig. 7 *X-Y* plane projection of the geometric trajectory.

$\gamma(0) = 0$ deg path angle and $\psi(0) = 0$ deg heading. The final position is (161.8,64.2,0) km, with final speed $v(s_f) = 110$ m/s, path angle $\gamma(s_f) = 0$ deg and heading $\psi(s_f) = -20$ deg. The horizontal projection of the trajectory contains two constant-rate turning maneuvers. The atmospheric density data are taken from [21].

The control bounds are given as follows: the lift coefficient $C_L \in [-0.067, 1.9]$, the bank angle $\phi \in [-25, 25]$ deg. The maximum speed limit is 0.85 Mach, whereas the minimum speed limit is $v_{\min} = 60$ m/s (134.2 mph). The wing surface area is $S = 510.97$ m^2 and the mass is $m = 288,938$ kg. These data correspond approximately to a Boeing 747 aircraft. The aerodynamic parameters K and C_{D_0} are taken from [22]. These Mach-dependent parameters are stored in look-up tables for computation. The dependence of the maximum thrust $T_{\max}$ (N) on the altitude z and Mach number M is taken into account by the following formula:

$$T_{\max}(M, z) = (-0.007236z + 146.1968) \times (e^{-1.97967M+8.23} + 2133)\ \text{N}$$

which fits approximately to the JT9D-7F engine maximum thrust data for a total of four engines.Using the optimal time-parameterization method, the minimum-time speed profile $v^*(s)$ was computed following the approach developed in this paper and is shown in Fig. 8. The same profile in terms of time is shown in Fig. 9. To arrive at the final position in minimum time, the aircraft should fly as fast as possible, however, due to the limited acceleration and deceleration capability, the optimal velocity profile cannot stay at $v_{\max}$ all the time. Within $0 \leq s \leq 37$ km, the upper limit of the speed is higher than 260 m/s, but the aircraft cannot travel at this maximum speed because it would not be able to decelerate sufficiently fast, thus

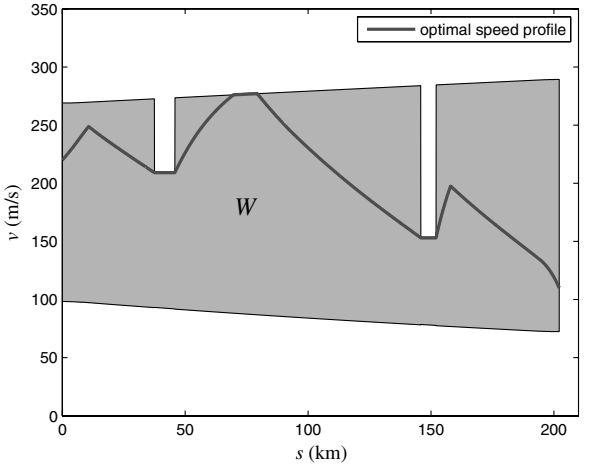

Fig. 8 Optimal speed profile under path coordinate.

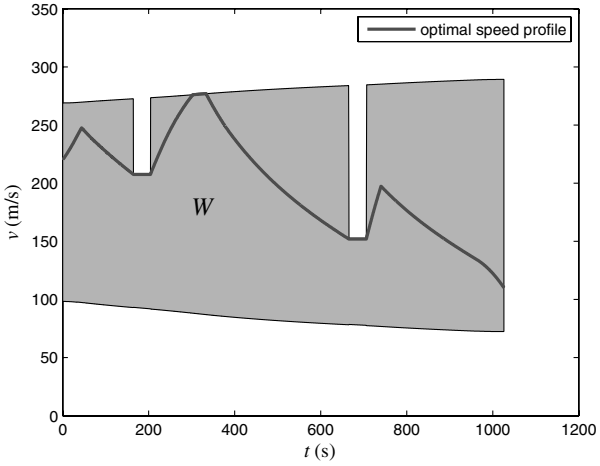

Fig. 9 Time history of optimal speed.

violating the speed upper limit within the interval $37 \le s \le 46$ km, which is induced by the first left turning maneuver. Similar scenarios exist before the second turning maneuver and the final point. The total length of the path is 202.2 km, and the aircraft finishes in 1021.9 s using the optimal thrust with an average speed of 197.9 m/s.

The state and control histories recovered from the optimally time-parameterized trajectory are shown in Figs. 10 and 11. As shown in the figures, the thrust and bank angle saturate during some phases of the flight. The saturations of the bank angle are caused by the turning maneuvers. The saturation of the thrust leads to maximum acceleration, which improves optimality.

To check the validity of this result, inverse dynamics are used to recover the state and control histories from the optimal time-parameterized trajectory $(x^*(t), y^*(t), z^*(t))$. For the purpose of validation, after the control histories are calculated from inverse dynamics, they are used as control inputs to numerically simulate the trajectory from the given initial conditions. The new simulated trajectory $(\hat{x}, \hat{y}, \hat{z})$ is compared with (x^*, y^*, z^*) in Fig. 12.

The discrepancy between the simulated trajectory and the original input trajectory is estimated using the following relative error index:

$$\Delta_r = \max_t \sqrt{\left(\frac{\hat{x}(t) - x^*(t)}{\max_t x^*(t) - \min_t x^*(t)}\right)^2 + \left(\frac{\hat{y}(t) - y^*(t)}{\max_t y^*(t) - \min_t y^*(t)}\right)^2 + \left(\frac{\hat{z}(t) - z^*(t)}{\max_t z^*(t) - \min_t z^*(t)}\right)^2}$$

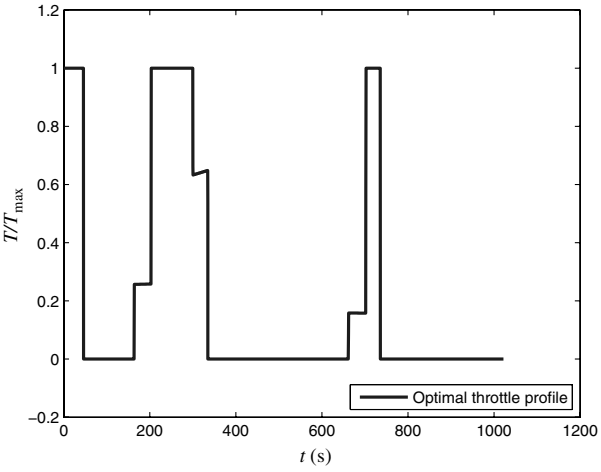

Fig. 10 Optimal thrust.

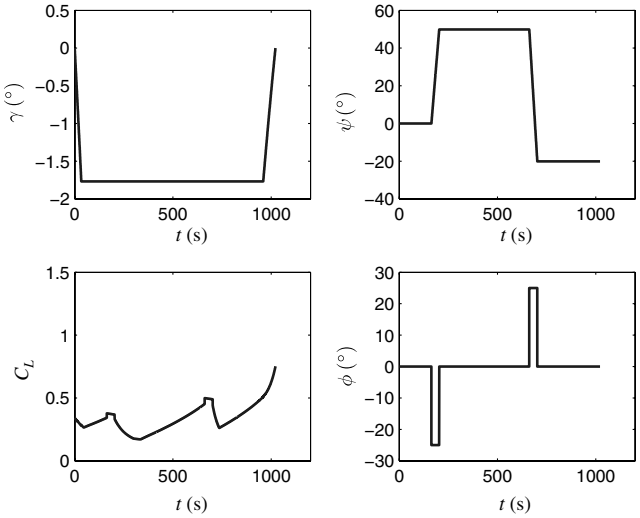

Fig. 11 States and control histories of the time-parameterized trajectory.

For this example, $\Delta_r = 7.1 \times 10^{-4}$, which is quite acceptable.

B. Time-Optimal Path

To validate the optimality of the time-parameterized trajectory, an already minimum-time landing path for a large civil aircraft was used to test the proposed method. The path is generated using DENMRA, which is a numerical algorithm solving optimal control problems with an automatic multiresolution mesh refinement scheme [23]. The accuracy and robustness of the DENMRA have been demonstrated in the same reference.

The aircraft starts at an initial position of (0,0,10) km and lands at an airport with position $(130, -65, 0)$ km. The initial conditions are speed $v(0) = 200$ m/s, heading angle $\psi(0) = 0$ deg, and path angle $\gamma(0) = 0$ deg; the final conditions are speed $v(s_f) = 110$ m/s, heading angle $\psi(s_f) = 80$ deg, and path angle $\gamma(s_f) = -30$ deg. The aircraft considered in this example is a Boeing-747. During the whole flight, the following constraints need to be satisfied: $v \le 250$ m/s, $\phi \in [-25, 25]$ deg, $C_L \in [-0.31, 1.52]$, and

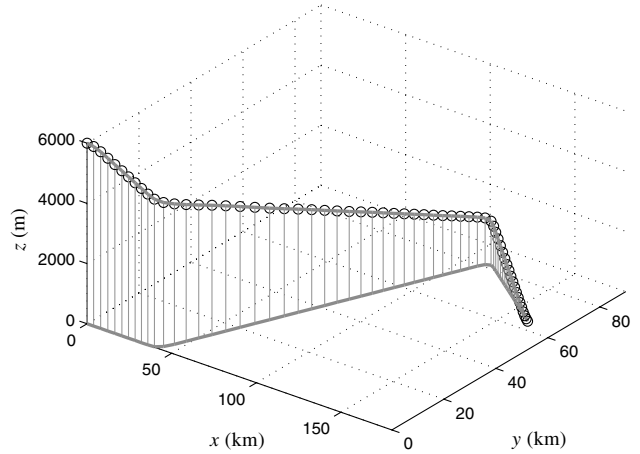

Fig. 12 Comparison of the original geometric path (dots) and the path generated using time parameterization and inverse dynamics (line).

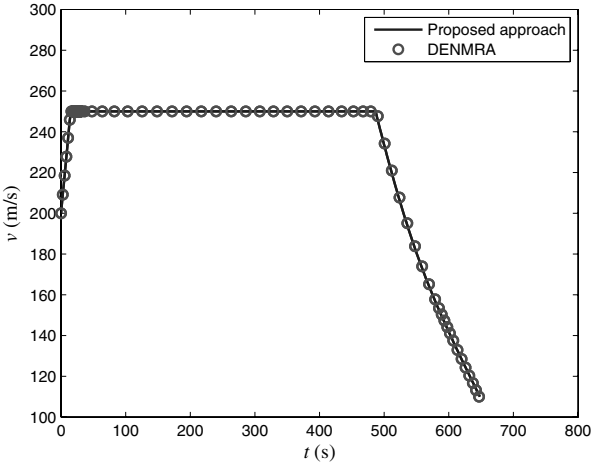

Fig. 13 Speed comparison.

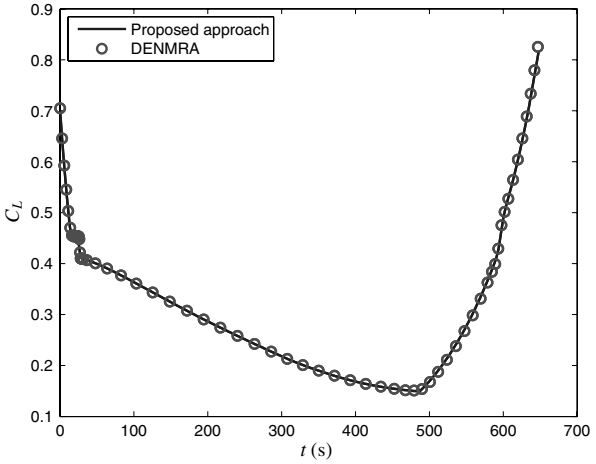

Fig. 14 Control comparison, C_L.

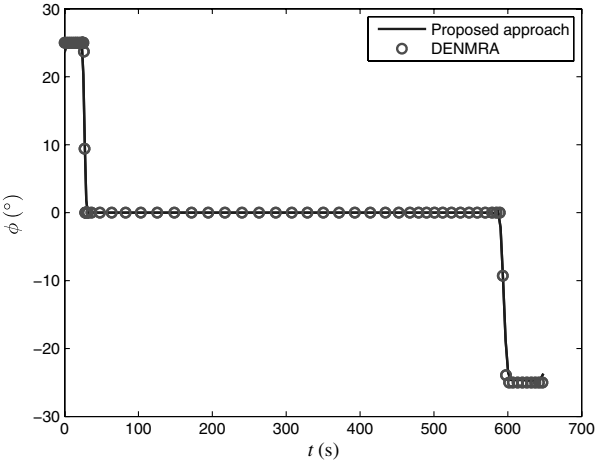

Fig. 15 Control comparison, ϕ.

$T \in [0, 1126.3]$ kN. Constant aerodynamic parameters $C_{D_0} = 0.0197$ and $K = 0.04589$ are used for this example to compute the optimal trajectory using DENMRA.

Because the state and control histories obtained from DENMRA are already time optimal, it is expected that the application of the time-parameterization method to the path corresponding to the DENMRA solution should yield the same optimal solution as that of DENMRA. The optimal parameterization method gives a total travel time of 548.0 s, which matches the final time of 546.9 s given by the DENMRA. The small discrepancy observed is attributed to the interpolation of the discrete path generated by the DENMRA and the numerical differentiation process required by the proposed method.

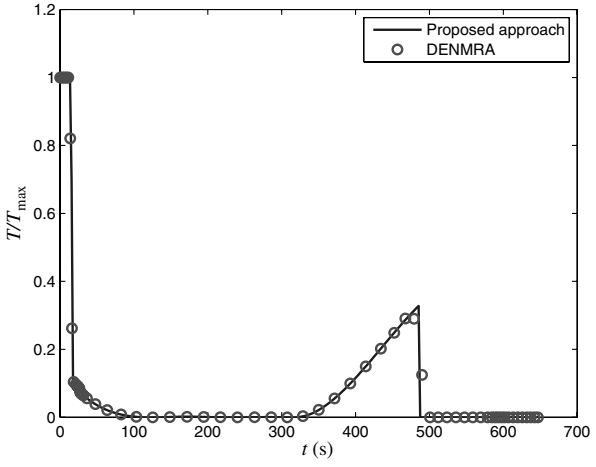

Fig. 16 Control comparison, throttle.

As shown in Figs. 13–16, the numerical optimization result agrees very well with that of the time-parameterization method. This agreement validates the optimality of the time-parameterization method and, to some extent, that of DENMRA as well.

VII. Conclusions

This paper studies the problem of minimum-time travel of a fixed-wing aircraft along a specified path. It has been proven that, within an interval in which the speed constraint is not active, there exists at most one switching, which is from maximum thrust to minimum thrust, hence the switching structure for the time-optimal control problem is unique. Constrained arcs riding on the upper bound of the admissible velocity can also be part of the optimal trajectory. The admissible specific kinetic energy set is used to characterize the domain within which the optimal specific kinetic energy profile is searched. The admissible specific kinetic energy set is generated by considering the constraints involving the aircraft speed and the remaining two controls, namely, the lift coefficient and the bank angle. Hence, a search within the admissible specific kinetic energy set naturally satisfies all state and control constraints. The optimal thrust history is then immediately determined from the optimal specific kinetic energy profile.

Two algorithms are proposed to solve for the thrust switching structure. The first algorithm can be implemented in parallel, which is difficult for other algorithms involving a sequential search, integrate, and check pattern. The second algorithm is based on the search, integrate, and check pattern, but improves its numerical efficiency by eliminating unnecessary integrations. Both algorithms are very efficient and are thus amenable to real-time implementation. These algorithms offer a computationally attractive alternative to the solution of the complete optimal control problem.

Tractability of the theoretical investigation of the optimal switching structure necessitates some simplifying assumptions on the aircraft dynamics, including small angle of attack and constant mass. Furthermore, the effects of speed brakes and the wind are not considered. In practical applications, the impact of these simplified assumptions needs to be evaluated.

Apart from a stand-alone approach for suboptimal minimum-time trajectory generation, the proposed method can also be used to construct good initial guesses for a generic trajectory optimization solver. Specifically, a geometric path can be optimally time parameterized to generate a feasible initial guess of the state and control histories, which can then be passed to the nonlinear programming solver as an initial guess for further improvement of the original path.

Finally, it is worth emphasizing that the proposed theoretical analysis is not intended as a substitute of purely numerical trajectory optimization approaches. The latter are unavoidable for high-fidelity trajectory generation. Rather, it is expected that the proposed theoretical analysis of a problem should be used hand-in-hand with solid and accurate numerical solutions to generate optimal trajectories in real time and with a high degree of confidence.

Acknowledgments

This work has been supported by NASA with contract NNX08AB94A, by NASA Ames Research Center.

References

[1] Miele, A., "Optimal Trajectories and Guidance Trajectories for Aircraft Flight Through Windshears," *Proceedings of the 29th IEEE Conference on Decision and Control*, Vol. 2, IEEE Publ., Piscataway, NJ, Dec. 1990, pp. 737–746.

[2] Lu, P., "Inverse Dynamics Approach to Trajectory Optimization for an Aerospace Plane," *Journal of Guidance, Control, and Dynamics*, Vol. 16, No. 4, 1993, pp. 726–732. doi:10.2514/3.21073

[3] Betts, J. T., and Cramer, E. J., "Application of Direct Transcription to Commercial Aircraft Trajectory Optimization," *Journal of Guidance, Control, and Dynamics*, Vol. 18, No. 1, 1995, pp. 151–159. doi:10.2514/3.56670

[4] Jacobsen, M., and Ringertz, U. T., "Airspace Constraints in Aircraft Emission Trajectory Optimization," *Journal of Aircraft*, Vol. 47, No. 4, 2010, pp. 1256–1265. doi:10.2514/1.47109

[5] Zhao, Y., and Tsiotras, P., "A Quadratic Programming Approach to Path Smoothing," *Proceedings of the American Control Conference*, American Automatic Control Council, Evanston, IL, 2011, pp. 5324–5329.

[6] Zhao, Y., "Efficient and Robust Aircraft Landing Trajectory Optimization," Ph.D. Thesis, School of Aerospace Engineering, Georgia Inst. of Technology, Atlanta, 2011.

[7] Nilsson, N. J., *Principles of Artificial Intelligence*, Tioga Publ., Palo Alto, CA, 1980, pp. 77–78.

[8] Stentz, A., "Optimal and Efficient Path Planning for Partially-Known Environments," *IEEE International Conference on Robotics and Automation*, IEEE Publ., Piscataway, NJ, 1994, pp. 3310–3317.

[9] Dubins, L. E., "On Curves of Minimal Length with a Constraint on Average Curvature, and with Prescribed Initial and Terminal Positions and Tangents," *American Journal of Mathematics*, Vol. 79, No. 3, 1957, pp. 497–516. doi:10.2307/2372560

[10] Chuang, J., and Ahuja, N., "Path Planning Using Newtonian Potential," *IEEE Conference on Robotics and Automation*, IEEE Publ., Piscataway, NJ, 1991, pp. 558–563.

[11] Bakolas, E., Zhao, Y., and Tsiotras, P., "Initial Guess Generation for Aircraft Landing Trajectory Optimization," *AIAA Guidance, Navigation, and Control Conference*, Portland, OR, AIAA, Reston, VA, 2011; also AIAA Paper 2011-6689.

[12] Petropoulos, A. E., and Longuski, J. M., "Shape-Based Algorithm for Automatec Design of Low-Thrust, Gravity-Assist Trajectories," *Journal of Spacecraft and Rockets*, Vol. 41, No. 5, 2004, pp. 787–796. doi:10.2514/1.13095

[13] Shiller, Z., and Lu, H.-H., "Computation of Path Constrained Time-Optimal Motions with Dynamic Singularities," *Journal of Dynamic Systems, Measurement and Control*, Vol. 114, No. 1, March 1992, pp. 34–40. doi:10.1115/1.2896505

[14] Bobrow, J. E., Dubowsky, S., and Gibson, J. S., "Time-Optimal Control of Robotic Manipulators Along Specified Paths," *International Journal of Robotics Research*, Vol. 4, No. 3, 1985, pp. 3–17. doi:10.1177/027836498500400301

[15] Shin, K. G., and McKay, N. D., "Minimum-Time Control of Robotic Manipulators with Geometric Path Constraints," *IEEE Transactions on Automatic Control*, Vol. AC-30, No. 6, June 1985, pp. 531–541. doi:10.1109/TAC.1985.1104009

[16] Pfeiffer, F., and Johanni, R., "A Concept for Manipulator Trajectory Planning," *IEEE Journal of Robotics and Automation*, Vol. RA-3, No. 2, April 1987, pp. 115–123. doi:10.1109/JRA.1987.1087090

[17] Shiller, Z., "On Singular Time-Optimal Control Along Specified Paths," *IEEE Transactions on Robotics and Automation*, Vol. 10, No. 4, Aug. 1994, pp. 561–566. doi:10.1109/70.313107

[18] Krantz, S. G., and Parks, H. R., *Primer of Real Analytic Functions*, Birkhauser, Boston, 2002, p. 3, Chap. 1.

[19] Miele, A., *Flight Mechanics, Vol. I: Theory of Flight Paths*, Addison Wesley, Reading, MA, 1962, pp. 48–50.

[20] Dahlquist, G., and Björck, Å., *Numerical Methods in Scientific Computing: Volume I*, Society for Industrial and Applied Mathematics, Philadelphia, 2008, pp. 171–172.

[21] NASA, "Earth Atmosphere Model," http://www.grc.nasa.gov/WWW/K-12/airplane/atmosmet.html [retrieved Aug. 2009].

[22] Mair, W. A., and Birdsall, D. L., *Aircraft Performance*, Cambridge Aerospace Series, Cambridge Univ. Press, Cambridge, U.K., 1996, p. 255.

[23] Zhao, Y., and Tsiotras, P., "Density Functions for Mesh Refinement in Numerical Optimal Control," *Journal of Guidance, Control, and Dynamics*, Vol. 34, No. 1, 2011, pp. 271–277. doi:10.2514/1.45852